DOI: 10.1784/ndt2025.1b1

# Comparison of Laser Ultrasonic Testing and traditional Ultrasonic Testing

Benjamin van Elburg, William Kramer, Patrick H. Jansen
Royal Netherlands Aerospace Centre,
Marknesse, 8316 PR, The Netherlands
+31 88 511 4700
benjamin.van.elburg@nlr.nl

## Abstract

Ultrasonic inspection is a widely accepted method in the aerospace industry for detecting defects and characterizing materials. However, the traditional ultrasonic technique requires precise alignment and couplant between the ultrasonic scanner and the material, or even complete water immersion. This can be impractical and limits its application. Laser ultrasonics overcomes these inconveniences by generating and detecting ultrasonic waves by lasers. This enables fast contactless ultrasonic inspection without couplant or immersion.

While laser ultrasonic inspection has advantages over traditional ultrasonic inspection, the generated ultrasound is relatively broadband and its intensity is limited by the ablation threshold, i.e. the maximum laser energy without damaging the material. Therefore a comparative study between ultrasonics and laser ultrasonics was conducted on representative aerospace components, focusing on defect detectability, signal-to-noise ratios, and inspection speed. Laser ultrasonics is up to 10 times faster than traditional single element ultrasonics. Both techniques can easily discriminate defects of 0.25 inch, however laser ultrasonics is less suited for defect detection in thick (> 5 mm) components. Furthermore, the relaxed alignment conditions of laser ultrasonics allow for the fast inspection of complex-shaped components.

## 1. Introduction

Non-destructive testing (NDT) plays a crucial role in the aerospace industry by ensuring the integrity and reliability of materials and structures. Ultrasonic testing (UT) is a proven and reliable inspection technique, where transducers emit and receive ultrasonic waves to determine internal integrity. The technique relies on acoustic impedance matching between a transducer and the test specimen by a coupling medium, which can be limiting in certain applications.

In recent years, laser ultrasonic testing (LUT) has emerged as a promising alternative [1], offering a non-contact approach to generating and detecting ultrasonic waves. In LUT the transducer is replaced by a generation and sensing laser. A high energy pulsed laser generates ultrasonic waves in the component by local rapid expansion through the photothermal effect. The surface vibrations as a result of these waves are detected by a sensing laser using interferometric methods. The laser beams can be directed by a mirror system to scan a surface, where a traditional UT would require translation of the transducer.

While laser ultrasonics offers advantages such as contactless and high inspection speed, the question remains how the inspection results compares to traditional UT. In this paper, we present a comparative analysis of laser ultrasonics and traditional pulse-echo ultrasonics, with a focus on defect detectability, signal-to-noise ratio (SNR) of defects, and inspection speed on composite components. An automatic laser ultrasonic inspection system is also presented.

The paper is organized as follows: first the specifications of both laser ultrasonic and ultrasonic systems are given, followed by a description of the composite samples that were tested. Subsequent sections compare and discuss the inspection results obtained from both systems, demonstrate the potential of automatic laser ultrasonic inspection systems, and conclude with a summary of the key findings.

## 2. Materials and methods

### *2.1 The laser ultrasonic system*

The laser ultrasonic system is the HUPI (Hybrid Ultrasonic Propagation Imaging) system made by Space NDT (South Korea) and is shown in Fig. 1. The system has a linear mode, where a translation stage moves the laser beams, and an angular mode, where a mirror system steers the laser beams. Only the angular mode was used to obtain the results in this paper.

**Figure 1: The angular laser ultrasonic system. On the right side a green aiming laser is visible on the steering mirror.**

The Q-Switched generation laser within the system is the Sol 40W 1064nm (Bright Solutions, Italy) and the sensing laser is the VibroFlex QTec (Polytec, Germany) laser doppler vibrometer (LDV). The generation laser was used at a 100% power setting of 2 mJ per pulse at a pulse repetition frequency of 10 kHz. The measuring frequency band was set between 1 and 1.5 MHz, the sampling rate was 80 MHz and a total of 1000 samples were measured per location. The scan index in both directions was set at 0.5 mm for all samples. Each scan was repeated three times (unless indicated otherwise) to improve the SNR. The data was analysed in MATLAB (The Mathworks, USA).

### *2.2 The ultrasonic system*

Traditional ultrasonic testing was done with a model S618 C-scan system (Ultrasonic Sciences LTD., UK) using a 5 MHz (44% bandwidth at -6 dB) single element transducer (IM-5-19-F76, Imasonic, France). The transducer has a focal distance of 76 mm and all samples were placed at the focus of the transducer. The ultrasonic system was used in pulse-echo mode. Ultrasonic waves were generated by a 150 volt 100 ns square pulse. The receiver gain was set such that the maximum of the entire measured signal was at 80% of the measurement range. Signals were sampled at 250 MHz and a total of 3250 samples per trace were recorded. Again the data was analysed in MATLAB.

### *2.3 Sample 1*

Sample 1 is a carbon fibre reinforced plastic (CFRP) test panel with 3 stiffeners and is schematically shown in Fig. 2A and B. The sample is made of aerospace grade carbon fibres, HexPly M18-1 resin and a standard paint system used on military weapon systems (Aerodur 37047 CF primer and PUR-Declack topcoat).The sample has real and artificial defects consisting of low-velocity impact damages, interply delaminations in the skin, and disbonds. The low-velocity impact damages were created by a guided drop weight

device with an impactor with a hemispherical steel tup. The interply delaminations and disbonds were simulated by inserting Tygavac TFG 075/1 foils of different diameter (Fothergill Tygaflor Ltd., UK). The locations of the defects are shown in Fig. 2A. The defects have varying diameters and depths, which are listed in Fig. 2C.

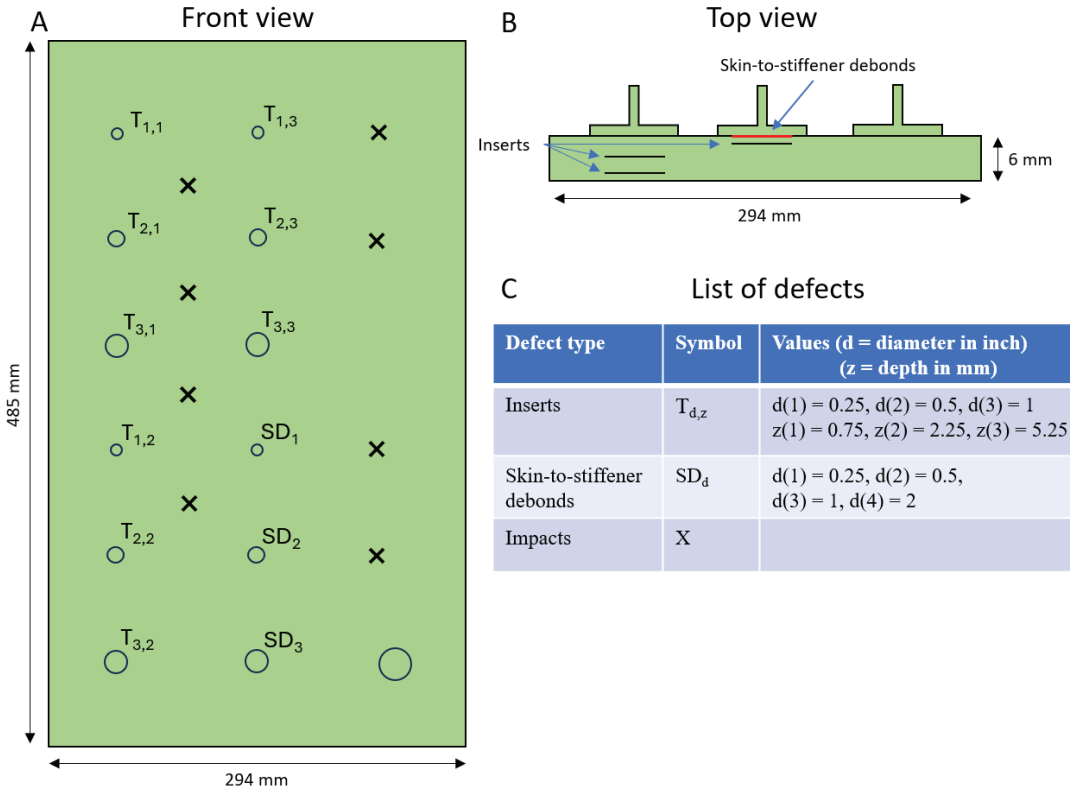


| Defect type | Symbol | Values (d = diameter in inch) (z = depth in mm) |
|---|---|---|
| Inserts | $T_{d,z}$ | d(1) = 0.25, d(2) = 0.5, d(3) = 1<br>z(1) = 0.75, z(2) = 2.25, z(3) = 5.25 |
| Skin-to-stiffener debonds | $SD_d$ | d(1) = 0.25, d(2) = 0.5,<br>d(3) = 1, d(4) = 2 |
| Impacts | X | |

**Figure 2: (A) A schematic drawing of the front view of sample 1 indicating the defect locations. (B) The top view. (C) A list of all the defects with their size and depth.**

### *2.4 Sample 2 and 3*

Sample 2 and 3 are made of the same materials as sample 1. Both samples have defects as shown on the schematic Fig. 3A. Sample 2 has a thickness of 2.7 mm and sample 3 has a thickness of 5.4 mm. The foils simulating delaminations were inserted at different depths for sample 2 and 3 as indicated in Fig. 3B and C.

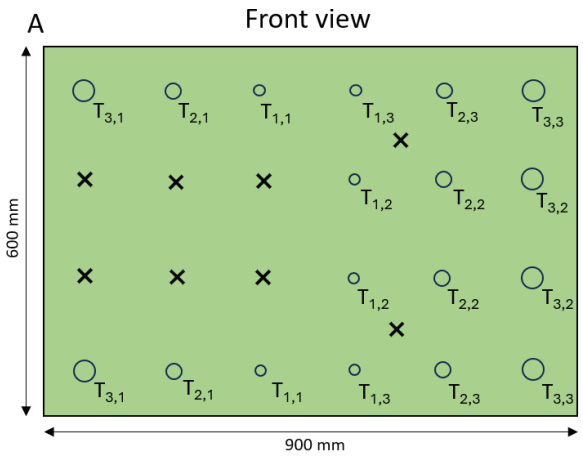


B Defects of sample 2

| Defect type | Symbol | Values (d = diameter in inch) (z = depth in mm) |
|---|---|---|
| Inserts | $T_{d,z}$ | d(1) = 0.25, d(2) = 0.5, d(3) = 1<br>z(1) = 0.7, z(2) = 1.4, z(3) = 2 |
| Impacts | X | |

C Defects of sample 3

| Defect type | Symbol | Values (d = diameter in inch) (z = depth in mm) |
|---|---|---|
| Inserts | $T_{d,z}$ | d(1) = 0.25, d(2) = 0.5, d(3) = 1<br>z(1) = 0.7, z(2) = 3.4, z(3) = 4.7 |
| Impacts | X | |

**Figure 3: (A) A schematic drawing of the front view of samples 2 and 3. Defects are located at the same locations on both samples. (B) A list of all the defects with their size and depth of sample 2. (C) A list of all the defects with their size and depth of sample 3.**

## 3. Results and discussion

### *3.1 Sample 1 UT vs LUT*

The measured radio frequency (RF) signals of the UT and LUT systems at 3 different locations of sample 1 are displayed in Fig. 4A and B, respectively. The three locations are a pristine spot, $T_{3,1}$ and $T_{1,2}$.

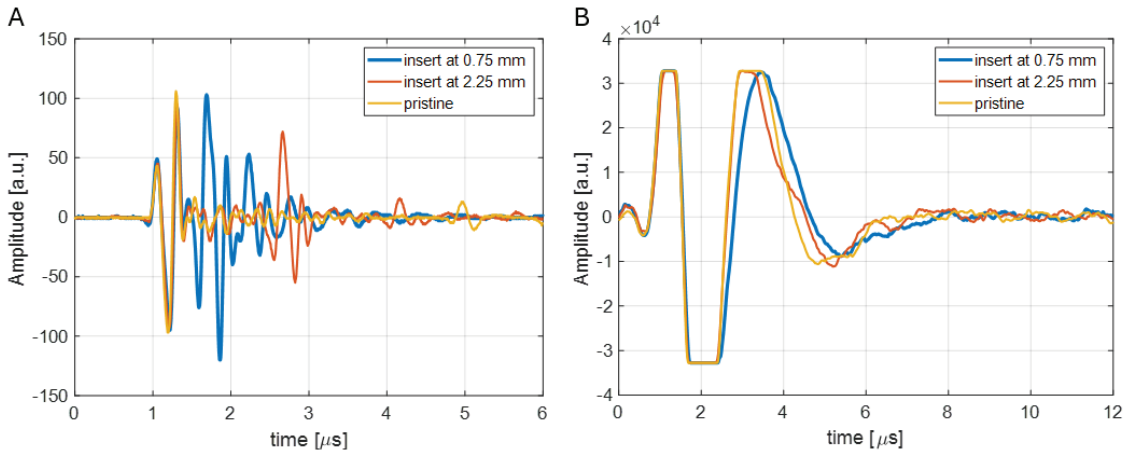


**Figure 4: (A) UT signals at a pristine spot and at two inclusions. (B) LUT signals at a pristine spot and at two inclusions.**

All three UT signals show a clear front wall reflection between 1 µs and 1.4 µs. The pristine signal has a back wall reflection at 5 µs, and little signal in between the front and back wall reflections, as the pristine material does not contain strong scatterers. In

contrast, a strong internal reflection can be seen at the locations with inserts. The blue curve, which is a signal obtained at a spot with an insert at a depth of 0.75 mm, has a strong refection between 1.5 and 2 μs. Similarly, the red curve has an echo between 2.5 and 3 μs. The reflection at a later time corresponds to the deeper insert at 2.25 mm.

The LUT signals in Fig. 4B differ significantly from the UT signals. The front wall echo is clipped by choice as the initial disturbance as a result of the generation pulse is large compared to internal reflections. There are differences in the signals at the end of the initial pulse for the different locations corresponding to the inserts. These small differences can be used to create a C-scan image in which the defects can be seen.

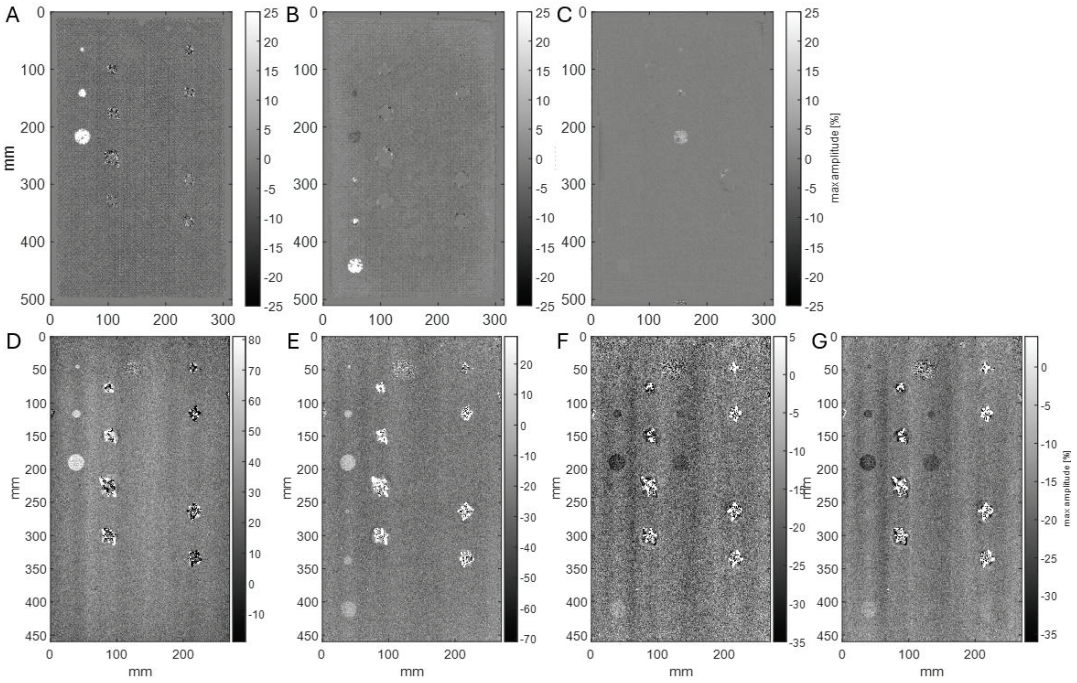


**Figure 5: (A-C) C-scan images of the ultrasonic data, where images are made using the amplitude at times that are optimized for the defects at 0.75, 2.25 and 5.25 mm. (D-F) ) C-scan images of the laser ultrasonic data, D, E and F are optimized for the depth of the defects. For G 10 repetitions were measured to increase the SNR.**

C-scan images for both the UT and LUT data are shown in Fig. 5. These images were made by displaying the amplitude of the RF signal at a certain time for all scan locations. Fig. 5A, B and C show UT C-scan images where the times (1.7, 2.7, and 4.7 μs) are optimized to visualize the inserts at a depth of 0.75, 2.25 and 5.25 mm, respectively. Similarly Fig. 5D, E and F show the LUT C-scan images at times 4.1, 4.5 and 5.9 μs. Fig. 5G uses the same time as Fig. 5F, however, for this result the LUT scan was repeated 10 times, instead of the standard 3 times, to increase the SNR.

On the UT C-scans, all inserts are clearly visible. Even the deepest and smallest 0.25 inch insert, $T_{1,3}$, is visible in Fig. 5C. The intensity of the reflection decreases with depth, which is visible as a decreasing the brightness in the image. However, compared to the background, the intensity remains sufficiently high to see the inserts. The impacts are visible in Fig. 5A because the impact damage is just beneath the skin, at a depth similar to the inserts. The skin-to-stiffener debonds do not show up in these images, but can be seen at the appropriate time index.

The scaling is different for each LUT C-scan image to improve visibility. On Fig. 5D all three inserts at a 0.75 mm depth are visible, as well as the impacts. Fig. 5E shows the inserts at a 2.25 mm depth, however the impacts and the inserts at a 0.75 mm depth are still visible. These inserts are visible because of the lower frequency (see Fig. 4B), and thus lower time resolution, of the LUT signal causing the reflections of the 0.75 and 2.25 mm deep inserts to overlap. The impacts are visible throughout the entire trace since the surface of the sample is deformed, which influences the coupling of the laser pulse and therefore results in a different signal, even at a later time. The deepest inserts can be seen in Fig. 5F, the 0.5 and 1 inch diameter inserts are somewhat visible, the 0.25 inch insert is invisible. Increasing the amount of repetitions from 3 to 10 (Fig. 5G) makes the inserts much more visible. The smallest insert, $T_{1,3}$, is obscured by a small surface area that was ablated by previous testing.

In order to quantify the results, the SNR of the defects was calculated by:

$$SNR\ (dB) = 20 * \log_{10} \frac{|A_{def} - A_{pris}|}{std(A_{pris})} \quad \ldots\ldots\ldots\ldots\ldots\ldots\ldots\ldots\ldots\ldots\ldots\ldots (1)$$

Here, $A_{def}$ is the average amplitude of 49 pixels within the defect area, $A_{pris}$ is the average amplitude of 441 pixels outside the defect area and $std(A_{pris})$ is the standard deviation of the 441 pristine amplitudes.

**Table 1. SNR and detectability for UT and LUT on sample 1**

| Defect group | SNR UT (dB) | SNR LUT (dB) | | detected | |
|---|---|---|---|---|---|
| | | 3x | 10x | UT | LUT |
| 0.75 mm depth inserts | 23.6 | 14.6 | 18.4 | 100 | 100 |
| 2.25 mm depth inserts | 24.0 | 9.0 | 13.8 | 100 | 100 |
| 5.25 mm depth inserts | 19.6 | <1 | 7.2 | 100 | 67 |
| Skin-to-stiffeners debonds (6 mm) | 14.4 | <1 | 7.0 | 100 | 50 |

The SNR and the percentage of detected defects per type are given in Table 1. The SNR listed is the average SNR of all the defects of the same type. The SNR confirms the results from the C-scan images. The UT results are clear for all the inserts and the skin-to-stiffener debonds (C-scan images not shown). A minor decrease in SNR can be seen for the defects that are deep within the sample. The LUT results show a strong decrease in

SNR with defect depth. For the 5.25 mm and deeper defects the SNR is below 1 and not all the defects can be seen. The SNR increases when more repetitions are measured, however the two smallest skin-to-stiffener debonds still cannot be detected.
While LUT performs worse than UT for defects that are 5.25 mm deep or deeper inside the CFRP sample, the major advantage is in the scanning speed. The scan time with UT was 36 minutes, the LUT scan (with 3 repetitions) took 3 minutes and 37 seconds, which is 10 times faster.

### *3.2 Sample 2 and 3 UT vs LUT*

The C-scan results for UT and LUT for sample 2 can be seen in Fig. 6A and B, respectively. The UT C-scan was made with a time gate in between the front and back wall echo, selecting the maximum of the signal's envelope. The LUT C-scan was made using a single time that optimized for all inserts.

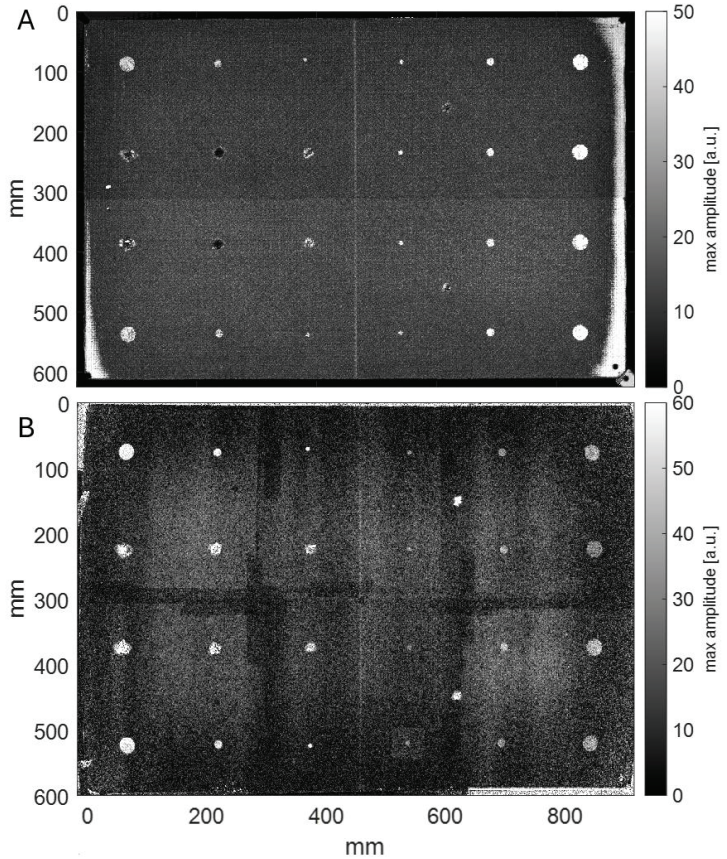


**Figure 6: The C-scans of sample 2 using (A) UT and (B) LUT. Both techniques find all defects.**

All inserts are visible in the thin CFRP sample on both the UT and LUT images. Note that the LUT data has dark rectangular markings, these are caused by tape residue that was

improperly removed. This highlights the photothermal interaction between the generation laser and the material compared to the pure ultrasonic interaction of the UT technique.
The lowest SNR of the inserts with UT was 13.9 dB with an average of 21.5 dB, while LUT resulted in an average SNR of 12.2, with the lowest SNR at 3.4 dB. The lowest SNR was at the smallest and deepest defects. While the LUT scan resulted in a lower SNR, all the defects could still be detected. The scan time was 13 minutes and 35 seconds for the LUT scan, while the UT scan took 1 hours and 49 minutes.
The C-scan results for UT and LUT for sample 3 can be seen in Fig. 7A and B, respectively. Again, using a time gate between the front wall and back wall echo all the defects can be visualized in a single C-scan for the UT data. The LUT image uses a time which was optimized for the deepest defects, however these are still invisible. The defects at 4.7 mm become visible by increasing the amount of repetitions to 10 as is shown in the small rectangular window in Fig. 7B.

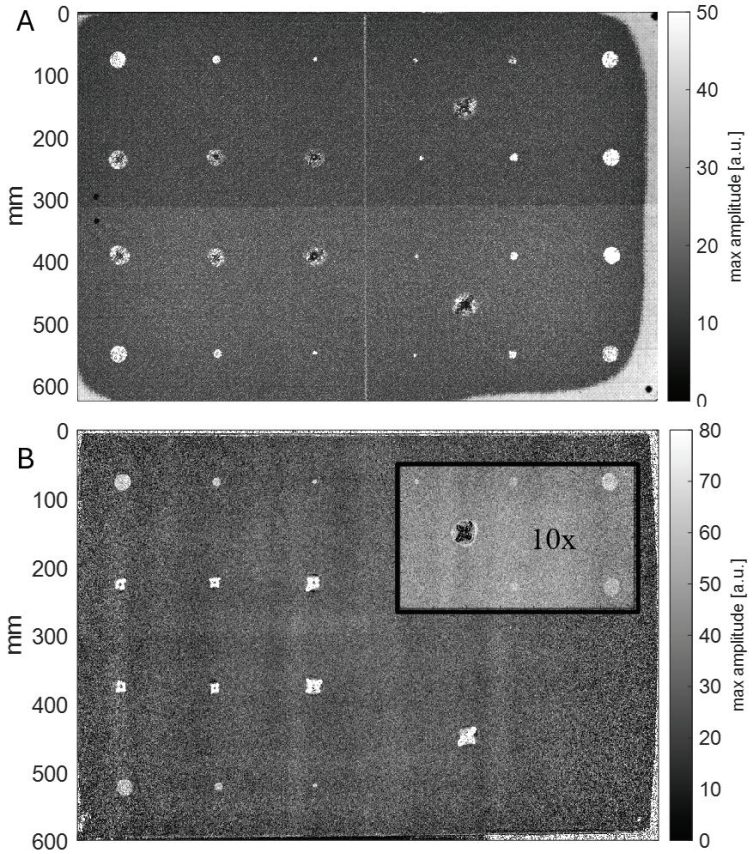


**Figure 7: The C-scans of sample 3 using (A) UT and (B) LUT.**

The average SNR of the defects on the UT image is 19.4 dB, with the lowest at 12.8 dB. For the LUT image only the inserts at 0.7 mm were detected with an average SNR of 10.4 dB. The inspection times for this sample are identical to sample 2.

## 4. The potential of laser ultrasonics inspection systems

The previous chapter compared UT and LUT on flat samples on a fundamental NDT basis for defect detection and inspection speed, however the working principle of LUT allows it to be used in a versatile manner with regards to curved composites.

### *4.1 Angle of incidence*

A traditional ultrasonic pulse echo measurement requires the transducer to be perpendicular to the surface. This requirement is less strict for laser ultrasonic testing as the sensing laser beam has a (partly) diffuse reflection on the surface. The accuracy of the LDV system as a function of stand-off distance and angle of incidence was tested with 3 different types of surfaces: shiny aluminium, matte aluminium and shiny CFRP composite. Testing was done by detecting the vibration of the front side surface of the test material. The vibration was constant and generated by a single element transducer placed on the backside of the test material. The maximum angle of incidence was determined by incrementally increasing the angle until the SNR sharply dropped.

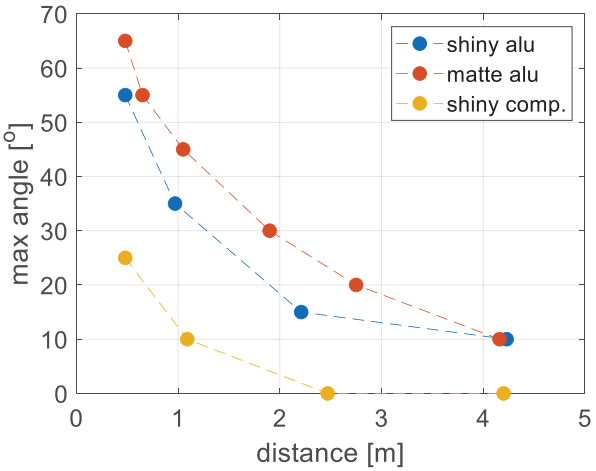


**Figure 8: The maximum angle of incidence at which the LDV can accurately measure.**

Fig. 8 shows the maximum angle of incidence for the 3 materials. The angle decreases with distance and differs per material. The shiny composite is the most sensitive to the angle of incidence, resulting in a 10 degree tolerance at a 1 meter stand-off distance. This allows the laser ultrasonic system to completely scan a composite component, curved in one direction, with 18 orientations. This, combined with the high scanning speed, makes laser ultrasonics ideal for fast inspection of curved composites.

### *4.2 Fast automated inspection system for curved composites*

A fast and automated inspection system for composites is presented here, that utilizes the long stand-off distance between component and scanner and the tolerance in angle of incidence of the LUT system. The system (Fig. 9) consists of a structured-light 3D scanner (Atos Core, Zeiss, Belgium), a software controlled rotation table with coded markers and the laser ultrasonic system.

**Figure 9: The automatic inspection system for curved composites with from left to right: the laser ultrasonic pc, the 3D scanner, the rotation table with a curved component, the laser ultrasonic scanner and the first author.**

The inspection system operates on the basis of the (coded) markers on the rotation table, which after an initial 3D scan form a digital point cloud on which the mesh of a component and the LUT results can be placed. The location of the laser ultrasonic scanner with respect to the point cloud is determined from a photograph made with a camera embedded within the scanner. The scanner location is determined using the coded markers on the photo. The automated system starts by making a mesh of the component with the 3D scanner, where the table rotates the component so it can be scanned from multiple angles. Then, a laser ultrasonic scan is made from a single angle, which is processed into a C-scan image. Fig. 10A shows a single C-scan image made of the curved part of a CFRP panel with a 160 degree curvature. On the inside of the panel, aluminium stickers have been placed as artificial defects. The single scan is able to detect the stickers in the middle of the scan area as the surface there is somewhat perpendicular to the scanner. However towards the sides, the image becomes noisy, because the angle of incidence increases beyond the tolerance of 10 degrees. Next, the process is repeated for in total 18 C-scans with 20 degree steps. Then, the noisy parts of the C-scan images are cut out. Finally, all the C-scan images are projected onto the mesh (Fig. 10B), resulting in a clear result over the entire curved surface (Fig. 10C).

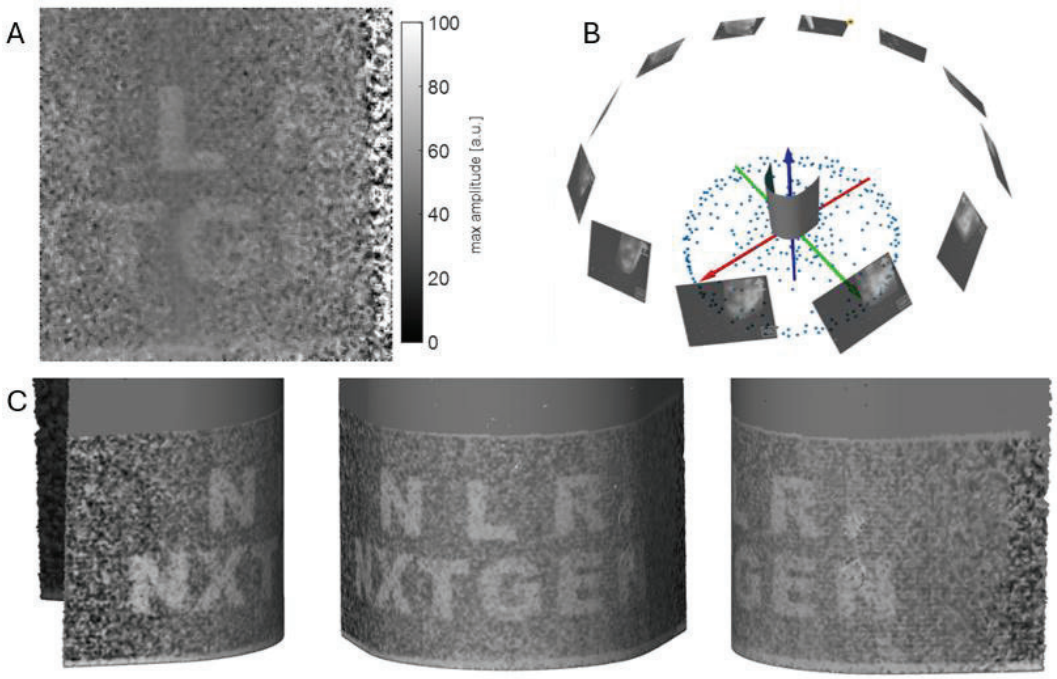


**Figure 10: (A) A single C-scan image of a curved component. (B) The point cloud, mesh and images. (C) All the scan results projected on the curved mesh.**

## 5. Conclusions

Laser ultrasonic testing is a promising alternative to ultrasonic testing. The defect detectability in composites is comparable for thin (<3 mm) components, but becomes significantly worse for thick (> 5 mm) components. This can be compensated to a certain degree by increasing the number of repetitions, which is feasible as 3 LUT scans are still 10 times faster than a single UT scan. The high scan speed, large tolerance in angle of incidence and the non-contact property of LUT make it an excellent NDT technique for a fast automated inspection system.

## 6. Funding

This research is made possible in part by a contribution from the Dutch National Growth Fund program NXTGEN Hightech.

## 7. Reference

1. A. Zarei, S. Pilla, ‘Laser ultrasonics for nondestructive testing of composite materials and structures: A review’, Ultrasonics, Volume 136, 2024.